Frontiers of Information Technology & Electronic Engineering
www.zju.edu.cn/jzus; engineering.cae.cn; www.springerlink.com
ISSN 2095-9184 (print); ISSN 2095-9230 (online)
E-mail: jzus@zju.edu.cn

Multiple target implementation for a doubly fed induction generator based on direct power control under unbalanced and distorted grid voltage*

Heng NIAN†‡, Yi-peng SONG

(*College of Electrical Engineering, Zhejiang University, Hangzhou 310027, China*)

†E-mail: nianheng@zju.edu.cn

Received May 8, 2014; Revision accepted Oct. 14, 2014; Crosschecked Mar. 6, 2015

Abstract: This paper presents a multiple target implementation technique for a doubly fed induction generator (DFIG) under unbalanced and distorted grid voltage based on direct power control (DPC). Based on the mathematical model of DFIG under unbalanced and distorted voltage, the proportional and integral (PI) regulator is adopted to regulate the DFIG average active and reactive powers, while the vector PI (VPI) resonant regulator is used to achieve three alternative control targets: (1) balanced and sinusoidal stator current; (2) smooth instantaneous stator active and reactive powers; (3) smooth electromagnetic torque and instantaneous stator reactive power. The major advantage of the proposed control strategy over the conventional method is that neither negative and harmonic sequence decomposition of grid voltage nor complicated control reference calculation is required. The insensitivity of the proposed control strategy to DFIG parameter deviation is analyzed. Finally, the DFIG experimental system is developed to validate the availability of the proposed DPC strategy under unbalanced and distorted grid voltage.

Key words: Direct power control, Doubly fed induction generator, Unbalanced and distorted grid voltage, Vector proportional and integral resonant regulator, Parameter deviation

doi:10.1631/FITEE.1400170 **Document code:** A **CLC number:** TM315

1 Introduction

Wind power generation systems based on a doubly fed induction generator (DFIG) have acquired increasing popularity all over the world due to the advantages of smaller converter rating, independent regulation of active and reactive powers, and lower converter cost and power losses compared with the fixed-speed induction generators or synchronous generators with full-sized converters. The control strategy of a DFIG system under an ideal power grid has been well investigated to satisfy the requirements of wind energy conversion and grid code (Iwanski and Koczara, 2008; Xu *et al.*, 2009; Luna *et al.*, 2011; Pena *et al.*, 2011; Cardenas *et al.*, 2013).

However, the practical power grid would always contain negative and harmonic voltage components, especially the 5th and 7th harmonic components. Thus, a severely unbalanced and distorted DFIG stator current would be produced. Currently, a grid operator always requires that the current injected by the renewable energy generation system should be balanced and sinusoidal, so that the power grid would not be further polluted. However, as the ratio of renewable energy including solar energy and wind energy becomes increasingly higher in power supply, the pulsation components of total active and reactive powers generated by the renewable power generation system will also be increasingly higher. This will be a potential

‡ Corresponding author

* Project supported by the National High-Tech R&D Program (863) of China (No. 2011AA050204) and the National Natural Science Foundation of China (No. 51277159)

ORCID: Heng NIAN, http://orcid.org/0000-0003-4816-084X

threat for the operational stability of power grid frequency and voltage. Even the safe and reliable operation of the power grid and renewable power generation system will be jeopardized. Therefore, to ensure reliable operation of the power grid and renewable energy generation system over the full range of operational conditions, the elimination of instantaneous active and reactive power fluctuation components at twice and six times the grid frequency is also chosen as a control target in this paper. Moreover, the DFIG electromagnetic torque pulsation caused by a non-ideal grid voltage would also be harmful to mechanical units, such as the gearbox and rotor bearing. It is essential to improve the DFIG control strategy to eliminate these detrimental influences.

Up to now, the control technique of DFIG under unbalanced grid voltage has been investigated to eliminate the harmful influence of the grid voltage negative sequence, that is, the unbalanced stator current, instantaneous stator active and reactive power pulsations, and electromagnetic torque pulsation (Xu and Wang, 2007; Hu and He, 2009; Hu *et al.*, 2009; Xu *et al.*, 2009; Nian *et al.*, 2011). On the other hand, when grid voltage distortion occurs, Liu *et al.* (2012), Xu *et al.* (2012a), and Nian and Song (2014) have presented a mathematical modeling and control strategy for DFIG under harmonically distorted grid voltage conditions, in which the alternative control targets were proposed to remove harmonically distorted stator current, restrain stator active and reactive power pulsations, or suppress electromagnetic torque pulsation. Furthermore, Xu *et al*. (2012b), Hu *et al.* (2013), and Martinez *et al.* (2013) investigated the DFIG control strategy under the unbalanced and harmonic grid voltage to achieve the sinusoidal and balanced stator current, eliminate the electromagnetic torque ripple, or eliminate the stator active power pulsation.

However, these studies (Xu and Wang, 2007; Hu and He, 2009; Hu *et al.*, 2009; Nian *et al.*, 2011; Xu *et al.*, 2012a; 2012b; Hu *et al.*, 2013; Martinez *et al.*, 2013; Nian and Song, 2014) were implemented based on the grid voltage negative and harmonic sequence decomposition. Then the inevitable phase delay and time delay due to the employment of the notch filters and low-pass filters would be introduced as a consequence, and the decomposition accuracy and system dynamic response would also deteriorate. Furthermore, the control reference calculation process is complicated and time-consuming. This process will also be unfavorable for digital implementation in practical applications.

To avoid harmonic decomposition and complicated reference calculation, an additional resonant closed-loop control of DFIG stator current was added in Liu *et al.* (2012), which can eliminate the harmonic components of the stator current under the harmonic grid voltage. Because neither harmonic decomposition nor rotor current reference calculation is needed, the dynamic performance of the DFIG system can be enhanced. However, the unbalanced grid condition was not considered in Liu *et al.* (2012), and the control target of smooth output power and smooth torque, which is a considerable factor in the reliable operation of a DFIG system, was also ignored.

To enhance the operation performance of DFIG under the condition of both grid voltage unbalance and harmonic distortion, direct power control (DPC) was implemented because of its advantage of DPC capability, simple implementation, and fast dynamic response (Zhou *et al.*, 2009; Nian *et al.*, 2011; Nian and Song, 2014). Moreover, vector oriented control (VOC) is a popular control strategy which has been widely adopted. Future work on improving the conventional VOC strategy can be expected. When DFIG works under the unbalanced and distorted grid voltage conditions, both conventional VOC and DPC would be inappropriate due to complicated negative and harmonic component extraction, as well as the time-consuming control reference calculation. Although grid voltage harmonic distortion was considered in the DFIG control based on DPC in Nian and Song (2014), only one control target of smooth active and reactive powers was introduced.

In this paper, the three alternative control targets can be implemented under the unbalanced and harmonic voltage conditions to achieve reliable and stable operation of the DFIG:

Target I: Balanced and sinusoidal stator current to ensure balanced heating and less harmonic loss in the three-phase stator winding, as well as to improve the power quality injected into the power grid.

Target II: Smooth stator active and reactive powers to ensure smooth wind energy injection into the power grid, which would be beneficial to safe and reliable grid operation.

Target III: Smooth electromagnetic torque to ensure reliable operation of the DFIG mechanical component, such as the gearbox and rotor bearing.

2 DFIG mathematical model under unbalanced and distorted grid voltage conditions

To investigate the proposed control strategy, a DFIG mathematical model under unbalanced and distorted grid voltage conditions should first be established. Given that the DFIG mathematical model has already been clearly established in Xu *et al*. (2012b) and Hu *et al*. (2013), it will only be briefly mentioned here.

Under the unbalanced and distorted grid voltage conditions, the grid voltage can be decomposed into fundamental, negative, and harmonic components. Since the major harmonic components of grid voltage are the 5th and 7th harmonic, this study focuses on the control strategy under negative and the 5th and 7th harmonic components. Fig. 1 shows the relationship among the fundamental, negative, and harmonic reference frames (ω_1 is the synchronous angular speed of the fundamental frequency grid voltage).

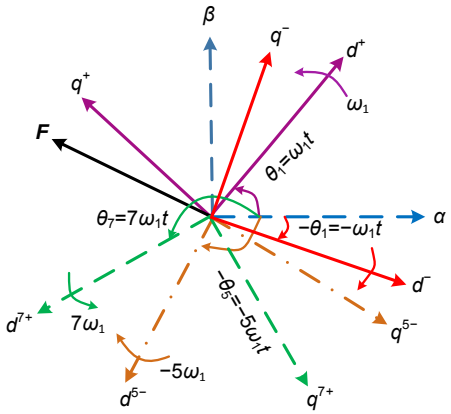

Fig. 1 Relationship among the reference frames $(dq)^+$, $(dq)^-$, $(dq)^{5-}$, and $(dq)^{7+}$

$(dq)^+$, $(dq)^-$, $(dq)^{5-}$, and $(dq)^{7+}$ are rotated at the speeds of ω_1, $-\omega_1$, $-5\omega_1$, and $7\omega_1$, respectively

According to Nian and Song (2014), the transfer function of the *d*-axis component of the rotor voltage (U_{rd}^+) to stator output active power (P_s) can be expressed as

$$\frac{P_s(s)}{U_{rd}^+(s)}=\frac{-3U_{sd}^+L_m/(2L_s)}{R_r+s\sigma L_r}, \tag{1a}$$

where R_r is the rotor resistance, L_m the mutual inductance, L_s the stator inductance, L_r the rotor inductance, U_{sd}^+ the *d*-axis component of grid voltage, and $\sigma=1-L_m^2/(L_sL_r)$ the leakage factor.

Similarly, the transfer function of the *q*-axis component of the rotor voltage (U_{rq}^+) to stator output reactive power (Q_s) can be expressed as

$$\frac{Q_s(s)}{U_{rq}^+(s)}=\frac{3U_{sd}^+L_m/(2L_s)}{R_r+s\sigma L_r}. \tag{1b}$$

The rotor voltages can be expressed as

$$\begin{aligned}U_{rd}^+&=V_{rd}^++E_{rd}^+\\&=-K(P_s^*-P_s)-\omega_s\left(\frac{Q_s}{k_\sigma U_{sd}^+}-\frac{L_rU_{sd}^+}{L_m\omega_1}\right),\end{aligned} \tag{2a}$$

$$U_{rq}^+=V_{rq}^++E_{rq}^+=K(Q_s^*-Q_s)-\omega_s\frac{P_s}{k_\sigma U_{sd}^+}, \tag{2b}$$

where V_{rd}^+ is the *d*-axis component of power regulator output, E_{rd}^+ the *d*-axis component of the direct power control decoupling compensation, V_{rq}^+ the *q*-axis component of power regulator output, E_{rq}^+ the *q*-axis component of the DPC decoupling compensation, P_s^* and Q_s^* the reference stator output active and reactive power respectively, ω_s the slip angular speed, and k_σ the leakage flux coefficient. K is used to represent the proper stator active and reactive power regulator for eliminating the power control error, which can be the proportional and integral (PI), proportional integral and resonant (PIR), or vector PI (VPI) regulator. It can be seen from Eqs. (2a) and (2b) that the rotor voltage reference consists of the stator active and reactive power regulator output (V_{rdq}^+) and the back electromagnetic force (E_{rdq}^+).

When grid voltage unbalance and harmonic distortion occur, the stator voltage contains not only fundamental, but also the negative and the 5th and 7th harmonic components, which will consequently cause

unbalanced and harmonic components in the stator current, and 100 Hz (interaction between fundamental and negative components) and 300 Hz (interaction between fundamental and the 5th and 7th harmonic components) pulsations in the instantaneous output active and reactive powers and electromagnetic torque of the DFIG. It should be noted that the 200 Hz (interaction between negative and the 5th harmonic components), 400 Hz (interaction between negative and the 7th harmonic components), and 600 Hz (interaction between the 5th and 7th harmonic components) pulsations can be neglected due to the relatively small amount of negative and the 5th and 7th harmonic components. Thus, these small pulsations will not be considered in the following discussions.

3 The proposed direct power control strategy

3.1 Conventional control strategy

Under the unbalanced and distorted grid voltage conditions, the control strategy based on the conventional VOC technique has been reported (Xu *et al*., 2012b; Hu *et al*., 2013) for DFIG operation. Moreover, conventional DPC techniques concerning unbalanced grid voltage (Zhou *et al.*, 2009; Nian *et al.*, 2011) or harmonic grid voltage (Nian and Song, 2014) have been covered. In these conventional VOC and DPC strategies, the grid voltage negative and harmonic components need to be decomposed and extracted by coordinate transformation and a notch filter. Then based on these decomposition results, the rotor current reference for the control targets I–III can be calculated. As a consequence, there are two major drawbacks of previous work:

1. Sequential decomposition of negative and harmonic components

The sequential decomposition process includes the coordinate transformation unit, and requires the accurate phase angle of the fundamental grid voltage, which is obtained through the phase locked loop (PLL). Thus, a slight grid voltage phase shift would reduce the accuracy of fundamental grid voltage phase angle, and have severe detrimental impact on the sequential decomposition accuracy as a consequence. Moreover, the decomposition would consume a large amount of digital signal processor (DSP) calculation time, and the filter would introduce phase delay, which will degrade the control performance in terms of speed and precision. Furthermore, the grid voltage negative sequence and harmonic components would always be on the dynamically various conditions, and thus the dynamic detection accuracy and system control performance can be jeopardized.

2. Complicated reference calculation

According to Xu *et al*. (2012a; 2012b) and Hu *et al.* (2009; 2013), the rotor current reference calculation in conventional VOC and the stator active and reactive power compensation calculation in conventional DPC (Zhou *et al.*, 2009; Nian *et al.*, 2011), would be indispensable and complicated. Additionally, considering that the DFIG parameters are involved when calculating the rotor current reference in VOC, as well as calculating stator active and reactive power compensation reference in DPC, DFIG parameter deviation due to temperature change and magnetic saturation would affect the accuracy of achieving the control targets.

Therefore, to simplify the control strategy configuration and improve DFIG operation capability, the above drawbacks are eliminated in our proposed control strategy. DPC rather than VOC is adopted due to its advantage of DPC capability, simple implementation, and fast dynamic response.

3.2 The proposed DPC strategy

The proposed DPC strategy with multiple control target implementation is shown in Fig. 2. Neither grid voltage negative nor harmonic decomposition is required, and complicated control reference calculation is not needed. Therefore, fast dynamic response and stable power control can be guaranteed for the specific control targets.

As shown in Fig. 2a, the proposed control strategy contains two independent closed control loops. One is the PI regulator to regulate the average component of stator active and reactive powers, so as to achieve the maximum power point track operation; the other is the VPI regulator to control the negative and harmonic components of the stator current, the 100 and 300 Hz fluctuant components of stator active and reactive powers, or the 100 and 300 Hz fluctuant components of electromagnetic torque and stator reactive power, so as to achieve the three alternative control targets. The three control targets can be achieved with the control configuration: since the

proposed DPC strategy is implemented in the $(dq)^+$ reference frame and all the three control targets are aimed at suppressing the detrimental 100 and 300 Hz components in the stator current, output power, or electromagnetic torque, the input reference of VPI regulator should be set at 0 to achieve the three alternative control targets.

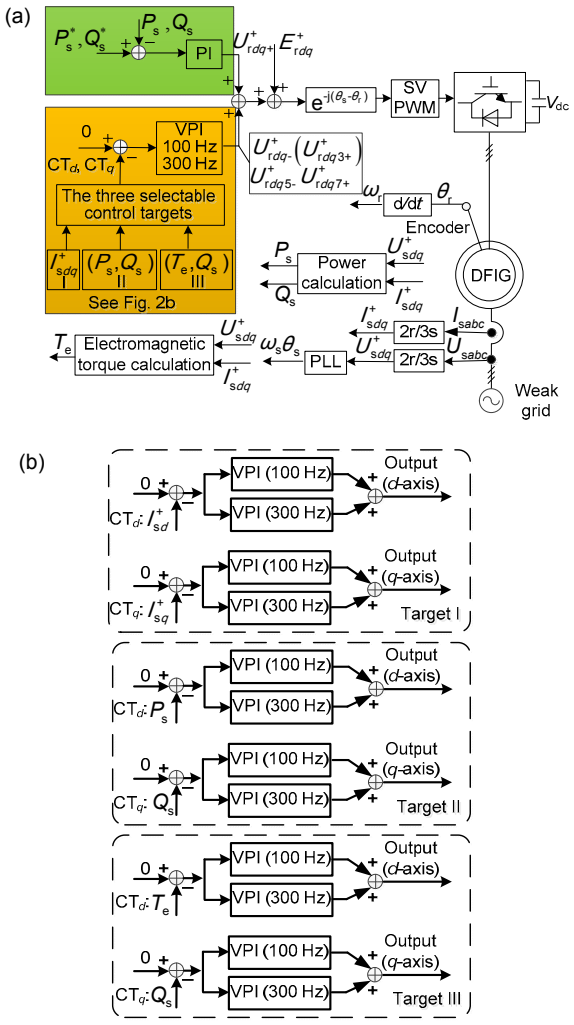

Fig. 2 Control scheme with the proposed control technique under unbalanced and distorted grid voltage conditions

(a) Block diagram of the proposed control strategy; (b) Detailed block diagram of the three control targets

1. Control target I: balanced and sinusoidal stator current

As shown in Fig. 2b, the stator current *d*- and *q*-axis components would be the *d*- and *q*-axis feedbacks of resonant closed-loop control. To eliminate the stator current negative and harmonic components, the VPI regulators would be tuned at 100 and 300 Hz, respectively. Therefore, the outputs in both *d*- and *q*-axis would contain the 100 and 300 Hz fluctuation components.

2. Control target II: smooth stator active and reactive powers

Similarly, to eliminate the stator power pulsation, the stator active power and reactive powers would be the *d*- and *q*-axis feedbacks of the resonant closed-loop control respectively, and the 100 and 300 Hz VPI regulators are adopted to suppress the power pulsation components.

3. Control target III: smooth electromagnetic torque and stator reactive power

Similarly, to remove the DFIG electromagnetic torque and stator reactive power pulsations, the electromagnetic torque and stator reactive power are chosen as the *d*- and *q*-axis feedbacks of resonant closed-loop control, and the 100 and 300 Hz VPI regulators are adopted to achieve smooth electromagnetic torque and stator reactive power.

The stator active and reactive powers and electromagnetic torque can be simply calculated as (Liu *et al.*, 2012)

$$P_\mathrm{s}+\mathrm{j}Q_\mathrm{s}=-\frac{3}{2}\boldsymbol{U}^+_{sdq}\hat{\boldsymbol{I}}^+_{sdq}, \tag{3a}$$

$$P_\mathrm{e}=\frac{3}{2}\omega_\mathrm{r}\,\mathrm{Re}[\mathrm{j}\boldsymbol{\psi}^+_{sdq}\hat{\boldsymbol{I}}^+_{sdq}], \tag{3b}$$

where P_e is the DFIG electromagnetic power, ω_r the rotor electrical angular speed, and $\boldsymbol{\psi}^+_{sdq}$ the stator flux.

Considering that I^+_{sdq}, P_s, Q_s, and T_e contain both the average DC and the 100 and 300 Hz AC components in synchronous frame $(dq)^+$, the VPI regulator should be tuned at 100 and 300 Hz respectively, to eliminate both the negative and harmonic components of the stator current, the 100 and 300 Hz stator active and reactive power pulsation, or the electromagnetic torque and 100 and 300 Hz stator reactive power pulsations. Furthermore, note that as the VPI regulator has high magnitude gain at 100 and 300 Hz and deep attenuation for the DC signal, only the 100 and 300 Hz AC components of the control error can be effectively regulated.

Thus, based on the above explanations, it can be seen that, to achieve the three control targets, no complicated control reference calculation or sequential decomposition is required in the proposed control strategy, which is beneficial for DFIG operation performance improvement and simple implementation.

The rotor control reference voltage can be deduced as follows:

$$U_{rd}^{+*}=V_{rd}^{+}+E_{rd}^{+}=-C_{\mathrm{PI}}(s)(P_{\mathrm{s}}^{*}-P_{\mathrm{s}}) -C_{\mathrm{VPI}}(s)(0-\mathrm{CT}_{d})-\omega_{\mathrm{s}}\left(\frac{Q_{\mathrm{s}}}{k_{\sigma}U_{sd}^{+}}-\frac{L_{\mathrm{r}}U_{sd}^{+}}{L_{\mathrm{m}}\omega_{\mathrm{l}}}\right), \quad (4a)$$

$$U_{rq}^{+*}=V_{rq}^{+}+E_{rq}^{+}=C_{\mathrm{PI}}(s)(Q_{\mathrm{s}}^{*}-Q_{\mathrm{s}}) +C_{\mathrm{VPI}}(s)(0-\mathrm{CT}_{q})-\omega_{\mathrm{s}}\frac{P_{\mathrm{s}}}{k_{\sigma}U_{sd}^{+}}, \quad (4b)$$

where P_{s}^{*} and Q_{s}^{*} are the stator active and reactive power references respectively, $C_{\mathrm{PI}}(s)$ the PI regulator transfer function, and $C_{\mathrm{VPI}}(s)$ the VPI regulator transfer function, which will be discussed in detail in Section 5. CT_d and CT_q are the d- and q-axis inputs of the VPI regulators respectively. I_{sd}^{+}, P_{s}, and T_{e} are for CT_d, and I_{sq}^{+} and Q_{s} for CT_q, according to the selected control target as shown in Fig. 2b. The last terms in both Eqs. (4a) and (4b) are the back electro-motive force (EMF) as compensation.

By integrating the PI closed-loop controller with the VPI resonant controller to implement the three alternative control targets for DFIG, the proposed DPC strategy has the following advantages over the conventional VOC and DPC strategies:

1. No sequence decomposition or complicated calculation

According to Fig. 2, the negative and the 5th and 7th harmonic decomposition and reference calculation are avoided, which would be quite helpful in reducing calculation time and improving the dynamic performance of DFIG under the unbalanced and harmonic voltage conditions.

2. No influence of DFIG parameter deviation on the accuracy of the control targets

Fig. 2 indicates that the proposed strategy can directly regulate the stator current negative and harmonic components, the stator active and reactive power pulsations, and the electromagnetic torque pulsation by the VPI regulator, while the calculation of rotor current in the conventional VOC or the power reference in the conventional DPC is not required. Thus, the influence of DFIG parameter deviation on the accuracy of the control targets can be eliminated.

3.3 Analysis of the stator current 3rd harmonic component under control target II

In Xu and Wang (2007) and Nian *et al.* (2011), only the stator active power or reactive power pulsation could be eliminated under the unbalanced voltage condition when the VOC is adopted. In this paper, the DFIG stator active and reactive power pulsations can be simultaneously removed under control target II at the cost of the occurrence of the stator current 3rd harmonic component. The proposed VPI regulator tuned at 100 Hz would produce an output signal of ±100 Hz in the reference frame $(dq)^{+}$, and the negative (−50 Hz) and the 3rd harmonic (+150 Hz) components of the stator current in a stationary frame will be introduced as a result. Thus, the 100 Hz stator output active and reactive power pulsation can be expressed as

$$\begin{aligned}P_{\mathrm{s}100}+\mathrm{j}Q_{\mathrm{s}100}&=-\frac{3}{2}(\boldsymbol{U}_{sdq-}^{-}\hat{\boldsymbol{I}}_{sdq+}^{+}\mathrm{e}^{-\mathrm{j}2\theta_{\mathrm{l}}}+\boldsymbol{U}_{sdq+}^{+}\hat{\boldsymbol{I}}_{sdq-}^{-}\mathrm{e}^{\mathrm{j}2\theta_{\mathrm{l}}} +\boldsymbol{U}_{sdq+}^{+}\hat{\boldsymbol{I}}_{sdq3+}^{3+}\mathrm{e}^{-\mathrm{j}2\theta_{\mathrm{l}}})\\&=-\frac{3}{2}[(k_1+k_3+k_5)\cos(2\theta_{\mathrm{l}})+(k_2-k_4+k_6)\sin(2\theta_{\mathrm{l}}) +\mathrm{j}(k_2+k_4+k_6)\cos(2\theta_{\mathrm{l}})+\mathrm{j}(k_3-k_1-k_5)\sin(2\theta_{\mathrm{l}})],\end{aligned} \quad (5a)$$

where

$$\begin{cases}k_1=U_{sd-}^{-}I_{sd+}^{+}+U_{sq-}^{-}I_{sq+}^{+},\\k_2=U_{sq-}^{-}I_{sd+}^{+}-U_{sd-}^{-}I_{sq+}^{+},\\k_3=U_{sd+}^{+}I_{sd-}^{-}+U_{sq+}^{+}I_{sq-}^{-},\\k_4=U_{sq+}^{+}I_{sd-}^{-}-U_{sd+}^{+}I_{sq-}^{-},\\k_5=U_{sd+}^{+}I_{sd3+}^{3+}+U_{sq+}^{+}I_{sq3+}^{3+},\\k_6=U_{sq+}^{+}I_{sd3+}^{3+}-U_{sd+}^{+}I_{sq3+}^{3+},\end{cases} \quad (5b)$$

and we have

$$\begin{cases} P_{\mathrm{scos}2} = -\dfrac{3}{2}(k_1 + k_3 + k_5), \\ P_{\mathrm{ssin}2} = -\dfrac{3}{2}(k_2 - k_4 + k_6), \\ Q_{\mathrm{scos}2} = -\dfrac{3}{2}(k_2 + k_4 + k_6), \\ Q_{\mathrm{ssin}2} = -\dfrac{3}{2}(k_3 - k_1 - k_5). \end{cases} \tag{5c}$$

Thus, based on Eqs. (5b) and (5c), to restrain the 100 Hz stator output active and reactive power pulsations, there should be k_3=k_4=0, k_1+k_5=0, and k_2+k_6=0. Thus, the following conclusions can be obtained:

1. When k_3=k_4=0, it can be deduced that the stator current negative component (I^{-}_{sdq-}) is 0. Thus, no stator current unbalanced components would be injected into the power grid when the 100 Hz stator output active and reactive power pulsation is restrained to zero.

2. When k_1+k_5=0, it can be found that the *d*-axis component of the stator 3rd harmonic current is related only to the grid voltage unbalanced components and stator current fundamental components, i.e.,

$$I^{3+}_{sd3+} = -(U^{-}_{sd-}I^{+}_{sd+} + U^{-}_{sq-}I^{+}_{sq+}) / U^{+}_{sd+}. \tag{6a}$$

Similarly, when k_2+k_6=0, the *q*-axis component of the stator 3rd harmonic current can be expressed as

$$I^{3+}_{sq3+} = (U^{-}_{sq-}I^{+}_{sd+} - U^{-}_{sd-}I^{+}_{sq+}) / U^{+}_{sd+}. \tag{6b}$$

Therefore, to eliminate the DFIG 100 Hz stator output active and reactive power pulsations simultaneously, the 3rd harmonic component in the stator current would be produced to counteract the power pulsation caused by the grid voltage negative component and the stator current fundamental component. Therefore, the balanced heating in the DFIG stator three-phase winding can be ensured, but the grid may be further polluted due to injecting the 3rd harmonic current into the power grid. Importantly, note that unlike the conventional 3rd harmonic current, which is a zero sequence component and has the same phase angle as in the *abc* phases, the produced stator current 3rd harmonic component under control target II are a positive sequence, indicating the phase angle differing from each other by 120° in the *abc* phases. Thus, the stator current 3rd harmonic component can flow within the transformer and DFIG stator winding.

4 VPI regulator and the insensitivity of closed-loop performance using VPI regulator to DFIG parameter deviation analysis

To achieve stable control of the negative and harmonic components under the unbalanced and distorted grid voltage conditions, the VPI regulator, based on pole-zero cancellation to avoid the unexpected gain peak (Lascu *et al.*, 2007; 2009), is introduced to replace the conventional PIR regulator due to the adequate closed-loop phase margin and the accurate tracking of the AC signal. The insensitivity of the proposed control strategy to DFIG parameter deviation will also be investigated.

4.1 Brief introduction to the VPI regulator

Since the stator current negative and harmonic components, the pulsation of stator active and reactive powers, and electromagnetic torque all behave as 100 and 300 Hz pulsation components in the frame $(dq)^{+}$, the resonant frequency of the VPI regulator should be tuned at 100 and 300 Hz, respectively.

The transfer function of the VPI regulator was first brought up by Lascu *et al.* (2007; 2009), and the resonant bandwidth was introduced to the conventional VPI as conducted in Nian and Song (2014),

$$C_{\mathrm{VPI}}(s) = \frac{K_{\mathrm{pr}2}s^2 + K_{\mathrm{ir}2}s}{s^2 + \omega_{\mathrm{c}2}s + (\pm 2\omega_1)^2} + \frac{K_{\mathrm{pr}6}s^2 + K_{\mathrm{ir}6}s}{s^2 + \omega_{\mathrm{c}6}s + (\pm 6\omega_1)^2}, \tag{7}$$

where $K_{\mathrm{pr}2}$ and $K_{\mathrm{pr}6}$, $K_{\mathrm{ir}2}$ and $K_{\mathrm{ir}6}$ are the PI coefficients of the VPI regulator tuned at the 100 and 300 Hz resonant frequency respectively, and $\omega_{\mathrm{c}2}$ and $\omega_{\mathrm{c}6}$ are the bandwidths at the resonant frequency of 100 and 300 Hz respectively, normally between 10 and 20 rad/s (Nian and Song, 2014).

According to Lascu *et al.* (2007; 2009), the parameters $K_{\mathrm{pr}2}$ and $K_{\mathrm{pr}6}$, $K_{\mathrm{ir}2}$ and $K_{\mathrm{ir}6}$ should be specified according to the rule of pole-zero cancellation to obviate the unexpected peak. Thus, the following equations can be obtained according to the experimental DFIG parameters listed in Table 3:

$$K_{\mathrm{ir}2}=K_{\mathrm{ir}6}=157K_{\mathrm{pr}2}=157K_{\mathrm{pr}6}. \tag{8}$$

4.2 Insensitivity of the proposed control strategy to DFIG parameter deviation

In practice, the DFIG parameters would always be influenced by temperature changes, insulation conditions, magnetic saturation, etc. It is meaningful to discuss the operation performance of the proposed DPC strategy under DFIG parameter deviation. It can be seen from Fig. 2 that the achievement of the proposed control targets is determined by the resonant control loop performance. Therefore, the resonant control loop should be analyzed to investigate its insensitivity to closed-loop performance using a VPI regulator to DFIG parameter deviation, and the control target of balanced and sinusoidal stator current is selected as an example.

As can be seen from Eq. (1), the major parameters that decide the operation performance of DFIG are R_r, L_r, L_s, and L_m (due to $\sigma=1-L_m^2/(L_sL_r)$). The stator and rotor inductances can be expressed as

$$L_s=L_m+L_{\sigma s},\quad L_r=L_m+L_{\sigma r}, \tag{9}$$

where $L_{\sigma s}$ is the stator leakage inductance and $L_{\sigma r}$ the rotor leakage inductance.

Since the stator leakage and rotor leakage can be regarded approximately equal to L_σ, the stator and rotor inductances can also be considered equal. As the resonant frequency is comparatively large and $s\sigma L_r$ would be more important than R_r, only a typical deviation of ±20% of parameters L_m and L_σ will be considered in this discussion (Jabr and Kar, 2007).

The resonant controller tuned at the 100 and 300 Hz has the same inherent characteristic, so only the control performance at the 300 Hz resonant frequency will be analyzed for simplicity; the analysis and conclusion for 100 Hz resonant frequency are similar. Based on Eqs. (1) and (7)–(9), the closed-loop transfer function at the 300 Hz resonant frequency for the control target of sinusoidal stator current can be derived as

$$\begin{aligned}C_{\mathrm{cl\_300Hz}}(s)=&[3U_{sd}^{+}L_m(K_{\mathrm{pr6}}s^2+K_{\mathrm{ir6}}s)/(2L_s)]\\&\cdot\{(R_r+s\sigma L_r)[s^2+\omega_{c6}s+(\pm6\omega_1)^2]\\&+3U_{sd}^{+}L_m(K_{\mathrm{pr6}}s^2+K_{\mathrm{ir6}}s)/(2L_s)\}^{-1}.\end{aligned} \tag{10}$$

Fig. 3 shows the closed-loop magnitude and phase response at the resonant frequency of 300 Hz when DFIG parameter deviation occurs. When the mutual inductance (L_m) varies within ±20%, the magnitude response remains almost constant (Fig. 3a). However, when leakage inductance (L_σ) varies within ±20%, comparatively large magnitude response changes can be observed. For instance, the maximum magnitude response of −0.595 dB can be obtained when both L_m and L_σ are 1.2 times the normal value, and similarly the minimum magnitude response of −0.876 dB when both L_m and L_σ are 0.8 times the normal value. Thus, the largest magnitude response variation would be 0.028 dB for the case of L_m and L_σ ±20% variation, which is negligible in practice and has no detrimental influence on the closed-loop steady-state control performance.

The closed-loop control phase response at resonant 300 Hz during DFIG parameter deviation can be obtained from Fig. 3b. The phase response at 300 Hz would be determined mainly by L_σ and is insensitive to L_m, which is similar to the result of Fig. 3a. A maximum phase response of 0.057° can be

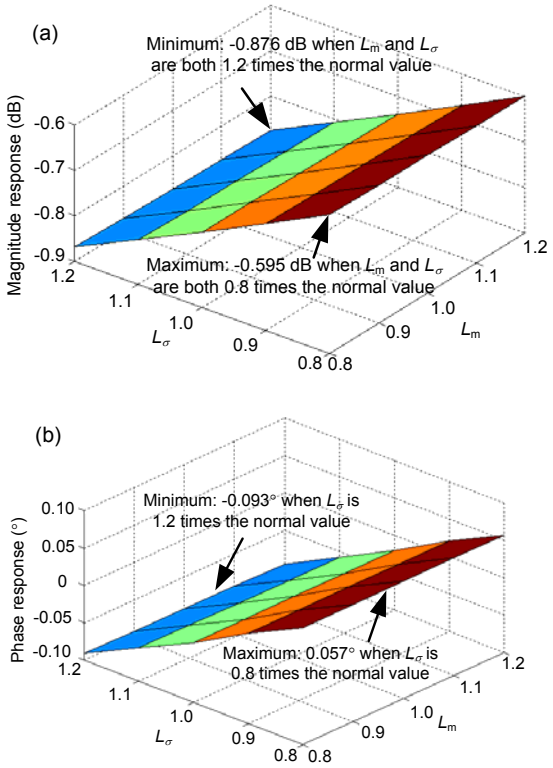

Fig. 3 Closed-loop magnitude (a) and phase (b) responses using the VPI regulator at resonant frequency 300 Hz
$\omega_{c2}=\omega_{c6}=15$ rad/s, $\omega_1=100\pi$ rad/s, $R_r=0.88$ Ω, $\sigma=0.06$, $L_r=0.093$ H, $k_{pr2}=k_{pr6}=1$, $k_{ir2}=k_{ir6}=157$

found when L_σ is 0.8 times the normal value, and the minimum phase response of −0.093° can be found when L_σ is 1.2 times the normal value. Thus, the largest phase response variation would be 0.15° for the case of L_m and L_σ ±20% variation, which is also small enough to be ignored in practice. Regardless of DFIG parameter deviation, the accurate AC signal tracking at 300 Hz frequency can be ensured.

Based on the above, the proposed strategy using the VPI regulator can ensure stable and reliable closed-loop operation with the excellent AC signal tracking ability at the 100 and 300 Hz, which will guarantee the successful and accurate achievement of specific control targets. Moreover, the VPI regulator can ensure the insensitivity of the proposed control strategy to DFIG parameter deviation under the typical parameter deviation range of L_m and L_σ ±20%.

5 Simulation validation

To test the proposed control strategy on a 2 MW-rated DFIG system, a simulation validation was conducted, and the parameters of the simulated DFIG system are given in Table 1. During the simulation, the grid voltage negative and the 5th and 7th harmonic components were set as 3%, 3%, and 3%, respectively.

Fig. 4 gives the simulation results of steady state performance of DFIG when the three respective control targets are achieved. It is observed that during control target I, balanced and sinusoidal stator current can be achieved; namely the 5th harmonic is 0.41%, the 7th harmonic 0.46%, the negative sequence 0.31%, and the 3rd harmonic 0.37%. However, the obvious stator active and reactive power pulsations and the electromagnetic torque fluctuation would be produced. Namely, the 100 and 300 Hz stator active power pulsations would be 2.66% and 3.87% respectively, the 100 and 300 Hz stator reactive power pulsation would be 4.02% and 4.24% respectively, and the 100 and 300 Hz electromagnetic torque pulsations would be 4.01% and 1.41% respectively. Similarly, when the control target II was implemented, the smooth stator active and reactive powers could be obtained, while the unbalanced and distorted stator current, as well as the electromagnetic torque fluctuation, would be a consequence. The detailed analysis data can be found in Table 2. When the control target III is achieved, the electromagnetic torque and stator reactive power are able to maintain a constant level, while the stator active power pulsation becomes larger, and the stator current becomes unbalanced and

Table 1 Parameters of simulated DFIG system

Parameter	Value	Parameter	Value
Rated power	2 MW	L_m	2.55 mH
Stator voltage	690 V	$L_{\sigma s}$	0.08 mH
R_s	2.57 Ω	$L_{\sigma r}$	0.08 mH
R_r	2.88 Ω	Number of pole pairs	2

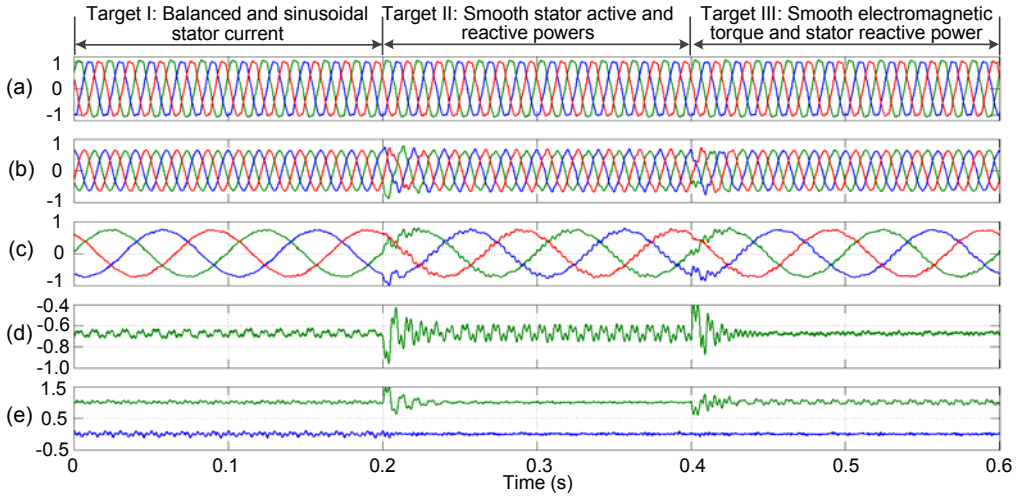

Fig. 4 Simulation results of steady state performance of DFIG when the three respective control targets are achieved
(a) Three-phase stator voltage (p.u.); (b) Three-phase stator current (p.u.); (c) Three-phase rotor current (p.u.); (d) DFIG electromagnetic torque (p.u.); (e) Stator active and reactive powers (p.u.)

distorted. The detailed analysis data is also available in Table 2.

Fig. 5 gives the simulation results of the DFIG stator active power stepping from 1.0 p.u. to 0.5 p.u. with the control target I. It is observed that both before and after the active power stepping moment, the stator current is able to maintain balance and sinusoidal stator current. Thus, the availability of the proposed control strategy can be validated. Moreover, the stator active power transient response time is around 20 ms, and no overshoot can be observed. Thus, it can be proved that the DPC using a PI regulator is able to quickly regulate the DFIG stator output active and reactive powers, and does not interfere with the proposed VPI closed-loop control strategy.

Table 2 Simulation analysis of the three control targets

Parameter	Target I	Target II	Target III
I_s (5th)	**0.41%**	1.65%	1.04%
I_s (7th)	**0.46%**	1.79%	1.04%
I_s (negative)	**0.31%**	1.21%	0.33%
I_s (3rd)	0.37%	1.59%	0.25%
P_s (100 Hz)	2.66%	**1.54%**	4.44%
P_s (300 Hz)	3.87%	**1.95%**	4.25%
Q_s (100 Hz)	4.02%	**2.29%**	**2.23%**
Q_s (300 Hz)	4.24%	**2.04%**	**2.01%**
T_e (100 Hz)	4.01%	5.23%	**2.25%**
T_e (300 Hz)	1.41%	2.97%	**0.80%**

Bold values are the minimum ones in the corresponding target

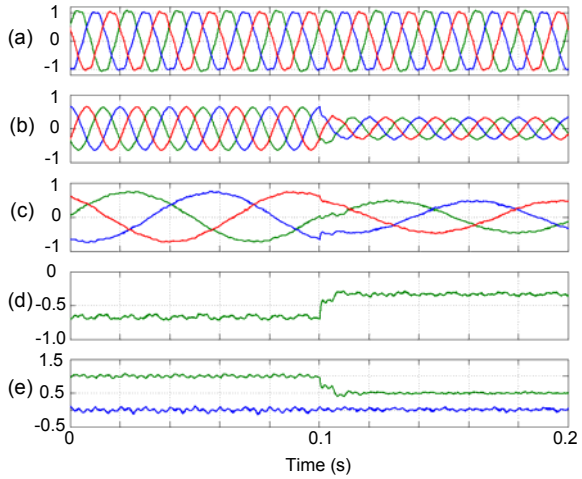

Fig. 5 Simulation results of DFIG stator active power stepping from 1.0 p.u. to 0.5 p.u. with control target I
(a) Three-phase stator voltage (p.u.); (b) Three-phase stator current (p.u.); (c) Three-phase rotor current (p.u.); (d) DFIG electromagnetic torque (p.u.); (e) Stator active and reactive powers (p.u.)

6 Experimental validation

6.1 Experimental setup

The experimental system was built on a laboratory prototype of a 1-kW DFIG system (Fig. 6), in which the DFIG was driven by a 1.5-kW squirrel cage induction machine acting as the wind turbine, and the induction machine was driven by a general converter. The rotor side converter of the DFIG was connected with a DC power supply, which acts as the grid side converter to provide a stable DC-link voltage. Chroma 61704 was used to simulate the practical unbalanced and distorted power grid. In the experiment, the negative and the 5th and 7th harmonic components of the grid voltage were set as 3.1%, 3.8%, and 2.5% respectively, and the rotor speed was initially set to be 800 r/min. All the control strategy was implemented on the TI DSP TMS320F2812, and the driver module for IGBT was SEMIKRON SKHI61. The sampling frequency was set to be 10 kHz, and the IGBT switching frequency was 5 kHz. The waveforms were acquired by a YOKOGAWA DL750 scope recorder, and the unbalanced and distorted component analysis was done by a FLUKE Norma 5000 power analyzer. Parameters of the experimental DFIG are listed in Table 3.

6.2 Results

During the experiment, a VPI regulator with resonant bandwidth $\omega_{c2}=\omega_{c6}=15$ rad/s was applied, together with the resonant parameters $K_{ir2}=K_{ir6}=1$,

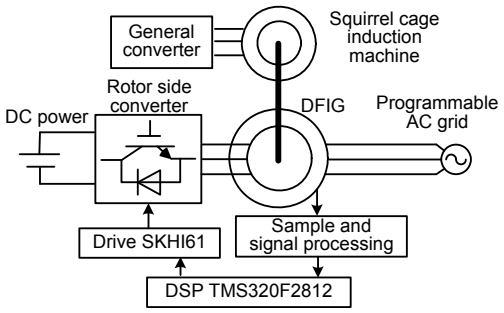

Fig. 6 Block diagram of the experimental system

Table 3 Parameters of the experimental DFIG system

Parameter	Value	Parameter	Value
Rated power	1 kW	L_m	90.1 mH
Stator voltage	110 V	$L_{\sigma s}$	2.83 mH
R_s	1.01 Ω	$L_{\sigma r}$	2.83 mH
R_r	0.88 Ω	Number of pole pairs	3

K_{pr2}=K_{pr6}=157, to follow the rule of pole-zero cancellation (Lascu *et al.*, 2007; 2009).

Fig. 7 shows the DFIG experimental results under an ideal power grid, which still contains a 0.25% negative component, 0.82% the 5th, and 0.65% the 7th harmonic component. Small non-sinusoidal components in the stator current, i.e., 2.51% the 5th and 1.41% the 7th harmonic component, can be found. Therefore, a small stator active and reactive power pulsation would be produced, of ±2.7 W at 100 Hz, ±1.5 W at 300 Hz, and ±1.6 var at 100 Hz, ±4.6 var at 300 Hz respectively, together with an electromagnetic torque pulsation of ±0.006 N·m at 100 Hz, and ±0.0065 N·m at 300 Hz.

Fig. 8 shows the results under unbalanced and distorted grid voltage conditions when the VPI controller is not enabled. It is observed that the heavily unbalanced and distorted stator current would occur with 5.88% negative, 7.00% the 5th, and 3.02% the 7th component. Furthermore, the 100 and 300 Hz pulsations of the stator active power are ±25 and ±6.6 W respectively, the 100 and 300 Hz pulsations of the stator reactive power are ±25 and ±11 var respectively, and the 100 and 300 Hz pulsations of the electromagnetic torque are ±0.105 and ±0.026 N·m, respectively. A detrimental DFIG system performance would be intolerable for the stable operation of the DFIG system under the unbalanced and distorted grid voltage conditions. The analysis of experimental data can also be found in the second column (no target) of Table 4.

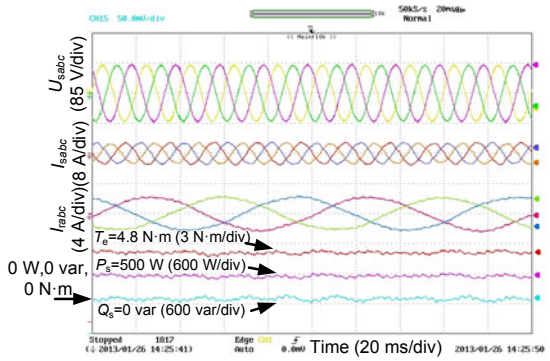

Fig. 7 Experimental results of DFIG system performance under an ideal grid voltage condition without a VPI regulator

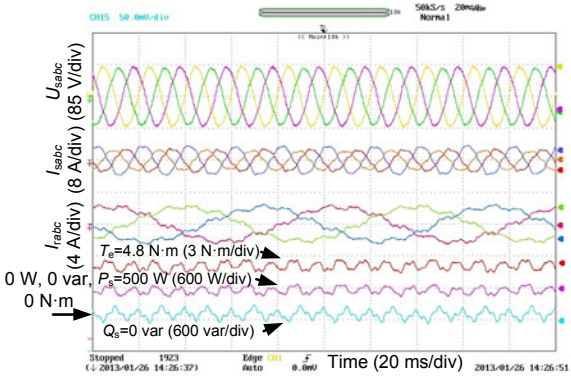

Fig. 8 Experimental results of DFIG system performance under unbalanced and distorted grid voltage conditions without target control

Table 4 Experimental analysis of the three control targets

Parameter	No target	Target I	Target II	Target III
I_s (5th)	7.00%	**2.19%**	2.27%	2.58%
I_s (7th)	3.02%	**1.29%**	1.68%	1.62%
I_s (negative)	5.88%	**0.39%**	0.21%	0.81%
I_s (3rd)	0.30%	0.34%	2.90%	0.26%
P_s (100 Hz) (W)	±25	±6.1	**±4.5**	±12
P_s (300 Hz) (W)	±6.6	±2.4	**±1.9**	±2.1
Q_s (100 Hz) (var)	±25	±4.3	**±4.3**	**±4.5**
Q_s (300 Hz) (var)	±11	±8.1	**±4.1**	**±3.8**
T_e (100 Hz) (N·m)	±0.105	±0.019	±0.032	**±0.015**
T_e (300 Hz) (N·m)	±0.026	±0.009	±0.015	**±0.006**

Bold values are the minimum ones in the corresponding target

Fig. 9 shows the results under unbalanced and distorted grid voltage conditions when the control target I is selected, and the data analysis can also be found in Table 4. When the VPI regulator tuned at the 100 and 300 Hz is used, the balanced and sinusoidal stator current can be achieved with 0.39% negative, 2.19% the 5th, and 1.29% the 7th component (Fig. 9a). Fig. 9b shows the transient response for the implementation of balanced and sinusoidal stator current. It is observed that before the control target enabling moment, there is an unbalanced and heavily distorted stator current. While after about 40 ms from the enabling, the stator current can be controlled to keep it balanced and sinusoidal, which verifies the fast and accurate regulation of the proposed DPC strategy with a VPI regulator.

Fig. 10 shows the results under unbalanced and distorted grid voltage when control target II is selected, and the data analysis can be found in Table 4. Fig. 10a shows that smooth stator active and reactive powers can be achieved, in which the 100 and 300 Hz

pulsations of the stator active power are ±4.5 and ±1.9 W respectively, and the 100 and 300 Hz pulsations of the stator reactive power are ±4.3 and ±4.1 var respectively. Nevertheless, 2.90% the 3rd harmonic component of the stator current can be found, which is significantly larger than the stator current 3rd harmonic component under targets I and III, while the stator current negative component would be 0.21%. The stator current 3rd harmonic component is generated to eliminate the 100 Hz pulsation of the stator active and reactive powers simultaneously, as discussed in Section 3.3. Furthermore, the transient response for the implementation of target II is shown in Fig. 10b. The active and reactive powers can be controlled to be smooth within 40 ms, which also validates the effectiveness of the proposed DPC strategy with a VPI regulator.

Fig. 11 shows the results under unbalanced and distorted grid voltage conditions when control target III is selected, and the data analysis can be found in Table 4. Fig. 11a shows that the smooth electromagnetic torque and stator reactive power can be achieved, in which the 100 and 300 Hz pulsations of electromagnetic torque are ±0.015 and ±0.006 N·m respectively, and the 100 and 300 Hz pulsations of stator reactive power are ±4.5 and ±3.8 var respectively. The transient experiment results, similar to Figs. 9b and 10b, are shown in Fig. 11b, which also validates the accurate and rapid tracking of the proposed DPC strategy with a VPI regulator.

Table 4 gives the data analysis and comparison of the different experimental results, including no control target and control targets I, II, and III. We achieved the best operational results always with a selected control target. For instance, when the control target of smooth stator active and reactive power is

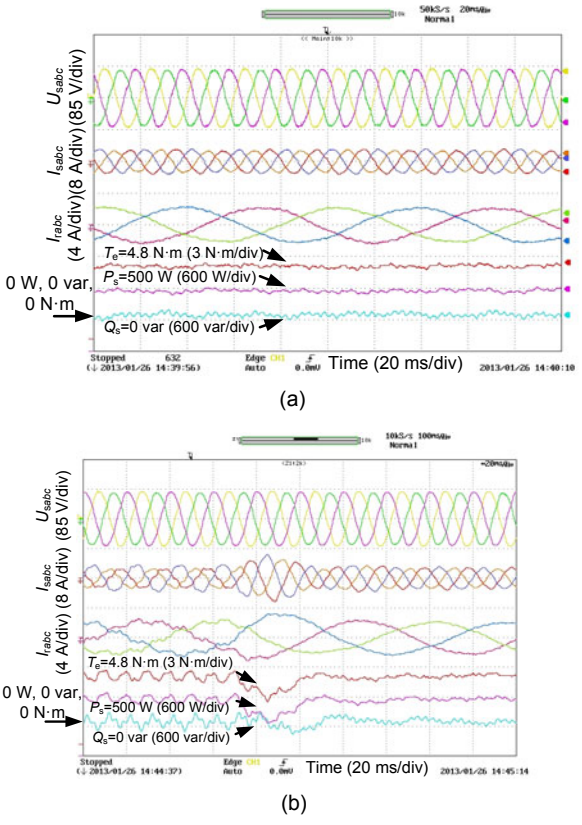

Fig. 9 Experimental results of DFIG system performance under unbalanced and distorted grid voltage conditions with control target I

(a) Steady state response; (b) Transient response of enabling stator current control

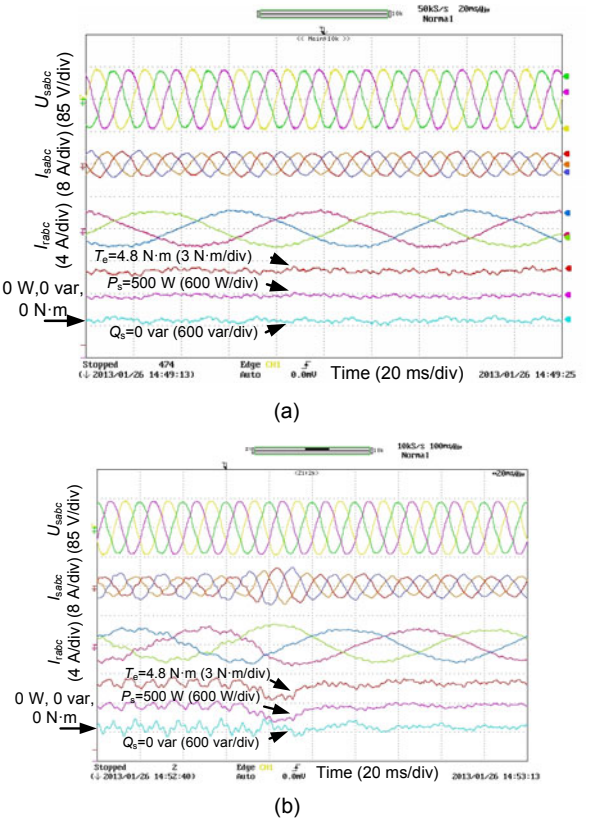

Fig. 10 Experimental results of DFIG system performance under unbalanced and distorted grid voltage conditions with the control target of smooth stator active and reactive powers

(a) Smooth stator active and reactive powers without 100 and 300 Hz pulsations; (b) Transient response of enabling stator active and reactive power control

chosen, the 100 and 300 Hz stator active and reactive powers would be ±4.5 W, ±1.9 W, ±4.3 var, ±4.1 var respectively, which are the minimum values among the results with all the three control targets (Table 4). A similar conclusion can be drawn for the other two control targets. Thus, the correctness and effectiveness of the proposed DPC strategy with a VPI regulator are well validated.

Fig. 12 shows the experimental results of transient response when the control target switches from smooth stator active and reactive power to balanced and sinusoidal stator current. It is observed that the transient response is very smooth without any observed impulse.

Fig. 13 shows the transient response of DFIG with stator active power reference stepping from 500 to 1000 W, and the control target is selected as smooth stator active and reactive power. It can be seen that the stator active power tracking error is relatively large at the moment of reference stepping. However, the active power control PI loop can regulate the stator active power following the reference signal within 30 ms, and the smooth stator power control target is also well achieved during the transient response.

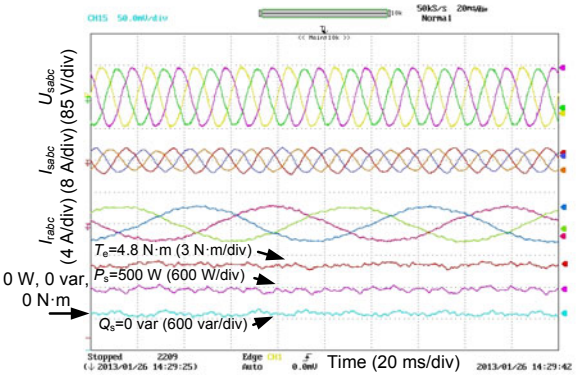

(a)

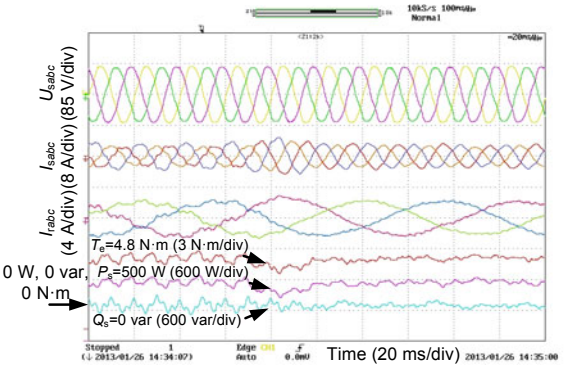

(b)

Fig. 11 Experimental results of DFIG system performance under unbalanced and distorted grid voltage conditions with control target III

(a) Smooth electromagnetic torque and stator reactive power without 100 and 300 Hz pulsations; (b) Transient response of enabling electromagnetic torque and stator reactive power control

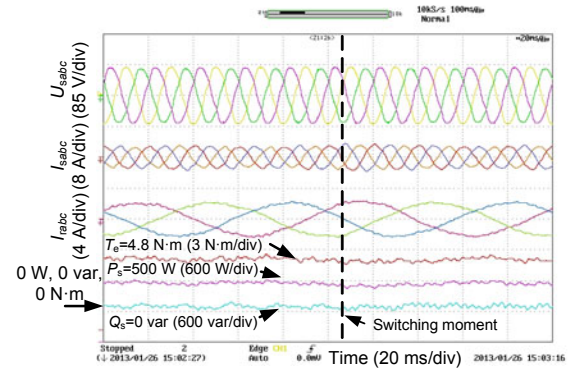

Fig. 12 Experimental results of DFIG system performance under unbalanced and distorted grid voltage conditions with control target switching from smooth stator active and reactive powers to balanced and sinusoidal stator current

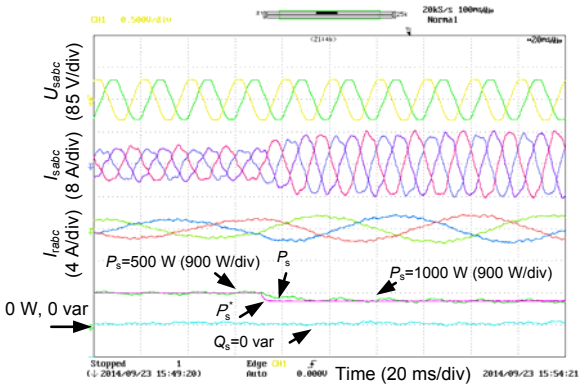

Fig. 13 Experimental results of DFIG system performance of stator active power reference stepping under unbalanced and distorted grid voltage conditions with the control target of stator active and reactive powers

7 Conclusions

This paper presents a multiple target implementation technique for DFIG under unbalanced and distorted grid based on DPC to achieve three alternative control targets: balanced and sinusoidal stator current, smooth stator active and reactive powers, and

smooth electromagnetic torque and stator reactive power. The experimental results validated the suitability of the proposed control strategy.

The major advantage of the proposed DPC strategy over conventional VOC and DPC strategies is that the need for a complicated and time-consuming grid voltage sequence decomposition and complicated reference calculation is eliminated, and thus faster dynamic response and more accurate steady state can be guaranteed. The proposed strategy, based on the VPI regulator tuned at 100 and 300 Hz resonant frequencies, is insensitive to DFIG parameter deviation.

When the control target II of smooth active and reactive powers is achieved, the stator current 3rd harmonic component occurs, while the stator current negative component is avoided. When the control target III is achieved, the electromagnetic torque and stator reactive power 100 and 300 Hz pulsations are eliminated simultaneously.

References

Cardenas, R., Pena, R., Alepuz, S., *et al.*, 2013. Overview of control systems for the operation of DFIGs in wind energy applications. *IEEE Trans. Ind. Electron.*, **60**(7): 2776-2798. [doi:10.1109/TIE.2013.2243372]

Hu, J., He, Y., 2009. Reinforced control and operation of DFIG-based wind-power-generation system under unbalanced grid voltage conditions. *IEEE Trans. Energy Conv.*, **24**(4):905-915. [doi:10.1109/TEC.2008.2001434]

Hu, J., He, Y., Xu, L., *et al.*, 2009. Improved control of DFIG systems during network unbalance using PI–R current regulators. *IEEE Trans. Ind. Electron.*, **56**(2):439-451. [doi:10.1109/TIE.2008.2006952]

Hu, J., Xu, H., He, Y., 2013. Coordinated control of DFIG's RSC and GSC under generalized unbalanced and distorted grid voltage conditions. *IEEE Trans. Ind. Electron.*, **60**(7):2808-2819. [doi:10.1109/TIE.2012.2217718]

Iwanski, G., Koczara, W., 2008. DFIG-based power generation system with UPS function for variable-speed applications. *IEEE Trans. Ind. Electron.*, **55**(8):3047-3054. [doi:10.1109/TIE.2008.918473]

Jabr, H.M., Kar, N.C., 2007. Effects of main and leakage flux saturation on the transient performances of doubly-fed wind driven induction generator. *Electr. Power Syst. Res.*, **77**(8):1019-1027. [doi:10.1016/j.epsr.2006.08.034]

Lascu, C., Asiminoaei, L., Boldea, I., *et al.*, 2007. High performance current controller for selective harmonic compensation in active power filters. *IEEE Trans. Power Electron.*, **22**(5):1826-1835. [doi:10.1109/TPEL.2007.904060]

Lascu, C., Asiminoaei, L., Boldea, I., *et al.*, 2009. Frequency response analysis of current controllers for selective harmonic compensation in active power filters. *IEEE Trans. Ind. Electron.*, **56**(2):337-347. [doi:10.1109/TIE.2008.2006953]

Liu, C., Blaabjerg, F., Chen, W., *et al.*, 2012. Stator current harmonic control with resonant controller for doubly fed induction generator. *IEEE Trans. Power Electron.*, **27**(7):3207-3220. [doi:10.1109/TPEL.2011.2179561]

Luna, A., Lima, F.K.A., Santos, D., *et al.*, 2011. Simplified modeling of a DFIG for transient studies in wind power applications. *IEEE Trans. Ind. Electron.*, **58**(1):9-20. [doi:10.1109/TIE.2010.2044131]

Martinez, M.I., Susperregui, A., Tapia, G., *et al.*, 2013. Sliding-mode control of a wind turbine-driven double-fed induction generator under non-ideal grid voltages. *IET Renew. Power Gener.*, **7**(4):370-379. [doi:10.1049/iet-rpg.2012.0172]

Nian, H., Song, Y., 2014. Direct power control of doubly fed induction generator under distorted grid voltage. *IEEE Trans. Power Electron.*, **29**(2):894-905. [doi:10.1109/TPEL.2013.2258943]

Nian, H., Song, Y., Zhou, P., *et al.*, 2011. Improved direct power control of a wind turbine driven doubly fed induction generator during transient grid voltage unbalance. *IEEE Trans. Energy Conv.*, **26**(3):976-986. [doi:10.1109/TEC.2011.2158436]

Pena, R., Cardenas, R., Reyes, E., *et al.*, 2011. Control of doubly fed induction generator via an indirect matrix converter with changing DC voltage. *IEEE Trans. Ind. Electron.*, **58**(10):4664-4674. [doi:10.1109/TIE.2011.2109334]

Xu, H., Hu, J., He, Y., 2012a. Operation of wind-turbine-driven DFIG systems under distorted grid voltage conditions: analysis and experimental validations. *IEEE Trans. Power Electron.*, **27**(5):2354-2366. [doi:10.1109/TPEL.2011.2174255]

Xu, H., Hu, J., He, Y., 2012b. Integrated modeling and enhanced control of DFIG under unbalanced and distorted grid voltage conditions. *IEEE Trans. Energy Conv.*, **27**(3):725-736. [doi:10.1109/TEC.2012.2199495]

Xu, L., Wang, Y., 2007. Dynamic modeling and control of DFIG-based wind turbines under unbalanced network conditions. *IEEE Trans. Power Syst.*, **22**(1):314-323. [doi:10.1109/TPWRS.2006.889113]

Xu, L., Zhi, D., Williams, B.W., 2009. Predictive current control of doubly fed induction generators. *IEEE Trans. Ind. Electron.*, **56**(10):4143-4153. [doi:10.1109/TIE.2009.2017552]

Zhou, P., He, Y., Sun, D., 2009. Improved direct power control of a DFIG-based wind turbine during network unbalance. *IEEE Trans. Power Electron.*, **24**(11):2465-2474. [doi:10.1109/TPEL.2009.2032188]